THE JOURNAL OF BIOLOGICAL CHEMISTRY
Vol. 274, No. 46, Issue of November 12, pp. 32680–32691, 1999
Printed in U.S.A.

Ruthenium Red Modifies the Cardiac and Skeletal Muscle Ca^{2+} Release Channels (Ryanodine Receptors) by Multiple Mechanisms*

(Received for publication, May 20, 1999, and in revised form, August 18, 1999)

Le Xu, Ashutosh Tripathy, Daniel A. Pasek, and Gerhard Meissner‡

From the Department of Biochemistry and Biophysics, University of North Carolina, Chapel Hill, North Carolina 27599-7260

The effects of ruthenium red (RR) on the skeletal and cardiac muscle ryanodine receptors (RyRs) were studied in vesicle-Ca^{2+} flux, [^{3}H]ryanodine binding, and single channel measurements. In vesicle-Ca^{2+} flux measurements, RR was more effective in inhibiting RyRs at 0.2 μM than 20 μM free Ca^{2+}. [^{3}H]Ryanodine binding measurements suggested noncompetitive interactions between RR inhibition and Ca^{2+} regulatory sites of RyRs. In symmetric 0.25 M KCl with 10–20 μM cytosolic Ca^{2+}, cytosolic RR decreased single channel activities at positive and negative holding potentials. In close to fully activated skeletal (20 μM Ca^{2+} + 2 mM ATP) and cardiac (200 μM Ca^{2+}) RyRs, cytosolic RR induced a predominant subconductance at a positive but not negative holding potential. Lumenal RR induced a major subconductance in cardiac RyR at negative but not positive holding potentials and several subconductances in skeletal RyR. The RR-related subconductances of cardiac RyR showed a nonlinear voltage dependence, and more than one RR molecule appeared to be involved in their formation. Cytosolic and lumenal RR also induced subconductances in Ca^{2+}-conducting skeletal and cardiac RyRs recorded at 0 mV holding potential. These results suggest that RR inhibits RyRs and induces subconductances by binding to cytosolic and lumenal sites of skeletal and cardiac RyRs.

The release and sequestration of Ca^{2+} ions by the sarcoplasmic reticulum (SR),[1] an intracellular membrane compartment, is essential to the process of cardiac and skeletal muscle contraction and relaxation. The rapid release of Ca^{2+} is mediated by Ca^{2+} release channels, also known as ryanodine receptors (RyRs), because they bind the plant alkaloid ryanodine with high affinity and specificity (1–6). Skeletal and cardiac muscles express two major isoforms of the RyR, RyR1 and RyR2, respectively. In striated muscles, RyRs are concentrated in the junctional SR membrane near transverse tubular, voltage-sensitive L-type Ca^{2+} channels (dihydropyridine receptors). A muscle action potential initiates dihydropyridine receptor conformational changes that activate the RyRs via a direct physical interaction in skeletal muscle or mediate the influx of Ca^{2+} in cardiac muscle, leading to the release of Ca^{2+} from the SR and subsequent muscle contraction. Both RyRs have been isolated as 30 S protein complexes composed of four 560-kDa (RyR polypeptide) and four 12-kDa (FK506-binding protein) subunits (1–5). The two channel activities are affected by endogenous and exogenous effectors, such as Ca^{2+}, Mg^{2+}, ATP, caffeine, ryanodine, and ruthenium red.

Ruthenium red (RR) is one of the most potent inhibitors of SR Ca^{2+} release (2). RR also inhibits mitochondrial Ca^{2+} uptake. However, this activity was due to a contaminant (7) that may be related to an oxygen-bridged R360 complex that, at concentrations as high as 10 μM, was without effect on SR Ca^{2+} uptake or release (8). RR is a polycationic dye with a linear structure consisting of three ruthenium atoms with a net valence of 6. In SR vesicles, RR increased the rate of Ca^{2+} uptake and decreased the rate of Ca^{2+} release at concentrations ranging from 1 nM to 20 μM (9–18). In muscle fibers, RR concentrations greater than 20 μM are required to inhibit SR Ca^{2+} release because of RR binding to myoplasmic proteins (19, 20). In intact single frog twitch muscle fibers, the estimated free RR concentration for half-block of SR Ca^{2+} release was 2.4 μM, in good agreement with the range reported for SR vesicle preparations (19). In [^{3}H]ryanodine binding measurements, RR decreased the B_{max} value and increased the K_D value, with the latter effect being due to a slower association rate (16). In single channel measurements, micromolar concentrations of RR decreased the channel open probability of the skeletal (21) and cardiac (22) RyRs by producing prolonged channel closings. A different effect was observed when ryanodine was used to lock the channels into a permanently open, Ca^{2+}-insensitive subconductance state. RR blocked single ryanodine-modified skeletal RyRs by binding in a voltage-dependent manner to multiple sites located in the conductance pore of the channel (23).

The present study was undertaken to clarify the effects of RR on ryanodine-unmodified skeletal and cardiac RyRs. The effects of RR on RyRs were investigated in SR Ca^{2+} uptake, [^{3}H]ryanodine binding, and single channel measurements using SR vesicles and purified cardiac and skeletal muscle RyRs. The results show that RR modifies the gating and conductance of the RyRs by multiple mechanisms, depending on channel activity, membrane potential, and sidedness of RR addition.

EXPERIMENTAL PROCEDURES

Materials—[^{3}H]Ryanodine was purchased from NEN Life Science Products. Unlabeled ryanodine was obtained from Calbiochem (San Diego, CA), ruthenium red was from Fluka (Ronkonkoma, NY), and phospholipids were from Avanti Polar Lipids (Alabaster, AL). Ryanodine and ruthenium red were prepared as concentrated stock solutions in 0.25 M KCl, 20 mM KHepes, pH 7.4, before their use. All other chemicals were of analytical grade.

Preparation of SR Vesicles and Purification of RyRs—"Heavy" rabbit

* This work was supported by National Institutes of Health Grants AR18687 and HL27430. The costs of publication of this article were defrayed in part by the payment of page charges. This article must therefore be hereby marked "*advertisement*" in accordance with 18 U.S.C. Section 1734 solely to indicate this fact.

‡ To whom correspondence should be addressed. Tel.: 919-966-5021; Fax: 919-966-2852; E-mail: meissner@med.unc.edu.

[1] The abbreviations used are: SR, sarcoplasmic reticulum; RyR, ryanodine receptor; RyR1, skeletal muscle RyR; RyR2, cardiac muscle RyR; RR, ruthenium red; P_o, channel open probability in the absence of a substate; P_{full}, open probability of full conductance events in the presence of a substate; P_{sub}, open probability of RR-related subconductances; P_{tot}, sum of P_{full} and P_{sub}; AMPPCP, adenosine 5′-(β,γ-methyleneriphosphate); CHAPS, 3-[(3-cholamidopropyl)dimethylammonio]-1-propanesulfonate.

skeletal and canine cardiac muscle SR membrane fractions enriched in [^{3}H]ryanodine binding and Ca^{2+} release channel activities were prepared in the presence of protease inhibitors (100 nM aprotinin, 1 μM leupeptin, 1 μM pepstatin, 1 mM benzamidine, 0.2 mM phenylmethylsulfonyl fluoride) as described (14, 24). The 3-[(3-cholamidopropyl)dimethylammonio]-1-propanesulfonate (CHAPS)-solubilized 30 S RyR complexes were isolated by rate density gradient centrifugation and reconstituted into proteoliposomes by removal of CHAPS by dialysis (25).

$^{45}Ca^{2+}$ Uptake Measurements—ATP-dependent $^{45}Ca^{2+}$ uptake by SR vesicles was determined using a filtration method. Samples were incubated for 1 h at 24 °C in 0.25 M KCl, 20 mM KHepes, pH 7.4, solutions containing 50 μM Ca^{2+}, 0.2 mM Pefabloc, and 20 μM leupeptin in the absence of ryanodine or the presence of 300 μM ryanodine to close the SR Ca^{2+} release channel (26–29). $^{45}Ca^{2+}$ uptake was initiated at 24 °C by the addition of 10 volumes of 0.25 M KCl, 20 mM KHepes, pH 7.4, solutions containing 5 mM MgATP, 5 mM NaN_3, 0.2 mM EGTA, various RR concentrations, and $^{45}Ca^{2+}$ to yield free Ca^{2+} concentrations of 0.2 and 20 μM. At various times, aliquots of the samples were placed on 0.45 μm Millipore filters under vacuum and rinsed with three 1-ml volumes of a 0.25 M KCl, 5 mM KPipes, pH 6.8, solution containing 0.1 mM EGTA, 10 mM Mg^{2+}, and 10 μM RR. Radioactivity remaining with the vesicles on the filters was counted by liquid scintillation.

[^{3}H]Ryanodine Binding—Unless otherwise indicated, SR vesicles were incubated for 20–24 h at 24 °C in 0.25 M KCl, 20 mM KHepes, pH 7.4, solutions containing 0.2 mM Pefabloc, 20 μM leupeptin, 1 nM [^{3}H]ryanodine, and various RR and free Ca^{2+} concentrations. Nonspecific [^{3}H]ryanodine binding was determined using a 1000-fold excess of unlabeled ryanodine. Aliquots of the samples were diluted with 10 volumes of ice-cold water and placed on Whatman GF/B filters soaked with 2% polyethyleneimine. Filters were washed with three 5-ml volumes of ice-cold 0.1 M KCl, 1 mM KPipes, pH 7.0. Radioactivity remaining with the filters was determined by liquid scintillation counting to obtain bound [^{3}H]ryanodine.

Hill constants (K_i) and coefficients (n_i) of [^{3}H]ryanodine binding inhibition by RR were determined using the following equation,

$$B = B_0/(1 + ([RR]/K_i)^{ni}) \quad \text{(Eq. 1)}$$

where B is [^{3}H]ryanodine binding at a given [RR], and B_o is the binding maximum in the absence of RR.

Single Channel Measurements and Analyses—Single channel measurements were performed by fusing proteoliposomes containing the purified RyRs with Mueller-Rudin type bilayers containing phosphatidylethanolamine, phosphatidylserine, and phosphatidylcholine in the ratio 5:3:2 (25 mg of total phospholipid per ml of *n*-decane) (30). The side of the bilayer to which the proteoliposomes were added was designated as the *cis* side. The *trans* side was defined as ground. Single channels were recorded in symmetric KCl buffer solutions (0.25 M KCl, 10–20 mM KHepes, pH 7.4) with additions as indicated in the text. Unless otherwise indicated, electrical signals were filtered at 2–4 kHz, digitized at 10–20 kHz, and analyzed as described (30). Data acquisition and analysis were performed using a commercially available software package (pClamp 6.0.3, Axon Instruments, Burlingame, CA) and an IBM-compatible computer (Pentium processor) with 12-bit analog/digital-digital/analog converter (Digidata 1200, Axon Instruments).

In the absence of RR-related subconductance states, channel open probability in the absence of a substate (P_o) was obtained by setting the threshold level at 50% of the current amplitude between the closed (*c*) and open (*o*) states. P_o values in multichannel recordings were calculated according to the equation $P_o = \Sigma\ iP_i/N$, where N is the total number of channels, and P_i is the i channel open probability. In some conditions, RR formed a predominant reduced conductance level (see Fig. 9*A, right panel, bottom trace, s*). RR formed additional subconductance states, but with some exceptions (see Figs. 6*D* and 7*B*), these occurred infrequently and were not further analyzed. The concentration and voltage dependence of the RR-related subconductances were obtained by determining the open probability of the full conductance events (P_{full}), RR-related subconductance events (P_{sub}), and the sum of P_{full} and P_{sub} (P_{tot}) (31). P_{full} was obtained by setting the threshold level at 50% current amplitude between subconductance (*s*) and open (*o*) current levels (see Fig. 9*A, right panel, bottom trace*). This measurement eliminated inclusion of substates in P_{full}. P_{tot} was obtained by setting the threshold level at 50% of the current between the close (*c*) and subconductance (*s*) current levels (see Fig. 9*A, right panel, bottom trace*). The open probability of the subconductance state, P_{sub}, was obtained by the equation $P_{sub} = P_{tot} - P_{full}$.

In the absence of substates, the Hill inhibition constant (K_i) and inhibition coefficient (n_i) of P_o were determined by the following equation,

$$P_0 = P_{0,max}/(1 + ([RR]/K_i)^{ni}) \quad \text{(Eq. 2)}$$

where $P_{o,max}$ is P_o in the absence of RR.

In the presence of substates, the Hill association constant (K_a) and coefficient (n_a) of P_{sub} state were determined by the following equation.

$$P_{sub} = P_{tot}/(1 + (K_a/[RR])^{na}) \quad \text{(Eq. 3)}$$

Assuming a Boltzman distribution between the P_{full} and P_{sub} states, their voltage dependence was described by the following equation,

$$P_{sub}/P_{full} = \exp[(Z_{tot}FV - G_i)/RT] \quad \text{(Eq. 4)}$$

where Z_{tot} is the effective gating charge of the reaction of RR with the RyR. The other terms have their usual meanings.

Determination of Free Ca^{2+} Concentrations—Free Ca^{2+} concentrations $\geq$1 μM were determined using a Ca^{2+} selective electrode (Nico Scientific, Philadelphia, PA). Free Ca^{2+} concentrations of $<$1 μM were obtained by including in the solutions the appropriate amounts of Ca^{2+} and EGTA as determined using the stability constants and the mixed solution program published by Schoenmakers *et al.* (32).

RESULTS

Effects of RR on $^{45}Ca^{2+}$ Uptake—The effects of RR on RyR ion channel activity were assessed in SR vesicle-$^{45}Ca^{2+}$ uptake measurements. Skeletal muscle SR vesicles of high buoyant density (previously designated heavy SR vesicles, Ref. 24) were actively loaded in 0.25 M KCl medium containing 0.2 μM (Fig. 1*A*) and 20 μM (Fig. 1*B*) free $^{45}Ca^{2+}$. The SR Ca^{2+} pump is present in these vesicles, but only 70–90% have RyR1 (24). To prevent release of sequestered $^{45}Ca^{2+}$, RyR1 was fully closed prior to $^{45}Ca^{2+}$ uptake by incubation for 1 h with 300 μM ryanodine (26–29). In the absence of RR, pretreatment with ryanodine increased the levels of $^{45}Ca^{2+}$ sequestered by the vesicles 3-fold in uptake medium containing 0.2 or 20 μM free Ca^{2+}. In ryanodine-untreated vesicles at 0.2 μM Ca^{2+}, 1 μM RR doubled the amount of $^{45}Ca^{2+}$ taken up by the vesicles. 10 μM RR was nearly as effective as pretreatment with ryanodine in increasing $^{45}Ca^{2+}$ uptake. By contrast, at 20 μM Ca^{2+}, 50 μM RR was required to achieve Ca^{2+} uptake levels approaching those observed in ryanodine-treated vesicles. RR did not increase $^{45}Ca^{2+}$ uptake by vesicles pretreated with ryanodine. For ryanodine-treated vesicles, a small decrease in the $^{45}Ca^{2+}$ uptake rate was observed in the presence of 50 μM RR, in agreement with the suggestion that high levels of RR inhibit the SR Ca^{2+} pump (33).

The effects of RR on Ca^{2+} uptake levels of ryanodine-treated and -untreated skeletal and cardiac SR vesicles were compared. $^{45}Ca^{2+}$ uptake levels were determined after an uptake period of 2 min. Cardiac SR contained a smaller proportion of vesicles responding to treatment with ryanodine (Fig. 2), in accordance with a 4–5-fold lower B_{max} value of [^{3}H]ryanodine binding for cardiac than skeletal SR vesicles (see Fig. 5). Ryanodine significantly increased $^{45}Ca^{2+}$ uptake or cardiac SR vesicles at 20 μM Ca^{2+} ($p < 0.05$; $n = 4$) but not at 0.2 μM Ca^{2+} ($p = 0.1$). In ryanodine-untreated SR vesicles, RR was more effective at 0.2 μM than at 20 μM Ca^{2+} in raising $^{45}Ca^{2+}$ uptake to levels in the ryanodine-treated vesicles. In agreement with previous vesicle ion flux measurements (9–18), the results indicate that the skeletal and cardiac muscle RyRs are inhibited by RR. The data in Fig. 2 further show that the extent of inhibition depends on the Ca^{2+} concentration of the uptake medium. Two possible reasons for this Ca^{2+} dependence are that SR Ca^{2+} pump activity is dependent on Ca^{2+} concentration and/or that Ca^{2+} ions compete with RR for the Ca^{2+} regulatory sites on the RyRs.

Effects of RR on [^{3}H]Ryanodine Binding to Skeletal and Cardiac Muscle SR Vesicles—The highly specific plant alkaloid

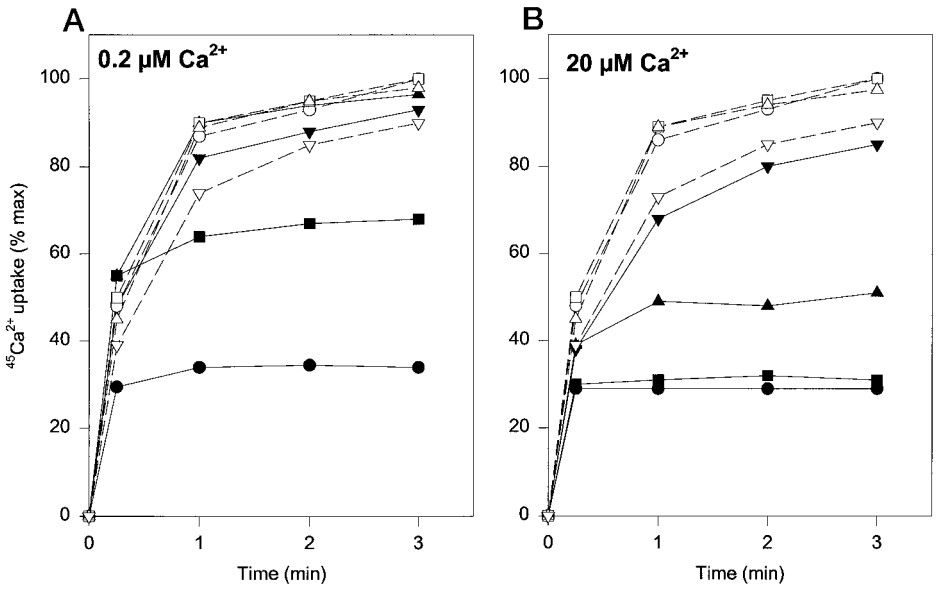

FIG. 1. **Effect of RR on $^{45}Ca^{2+}$ uptake by ryanodine-treated and -untreated heavy skeletal muscle SR vesicles.** ATP-dependent $^{45}Ca^{2+}$ uptake was determined by a filtration method as described under "Experimental Procedures." Samples were incubated in the absence (*filled symbols*) or the presence (*open symbols*) of 300 μM ryanodine before $^{45}Ca^{2+}$ uptake was initiated. $^{45}Ca^{2+}$ uptake medium contained 0.2 μM (*A*) or 20 μM (*B*) free Ca^{2+} and 0 (● and ○) 1 (■ and □), 10 (▲ and △), or 50 (▼ and ▽) μM RR. At various times, aliquots of the samples were placed on 0.45 μm Millipore filters under vacuum and rinsed with a 0.25 M KCl solution containing 0.1 mM EGTA, 10 mM Mg^{2+}, and 10 μM RR. The radioactivity remaining with the vesicles on the filters was determined. The maximum values (100% = maximum value for ryanodine-treated vesicles in the absence of RR) corresponded to 56 and 158 nmol of $^{45}Ca^{2+}$/mg of protein at 0.2 and 20 μM Ca^{2+}, respectively. One of three similar experiments is shown.

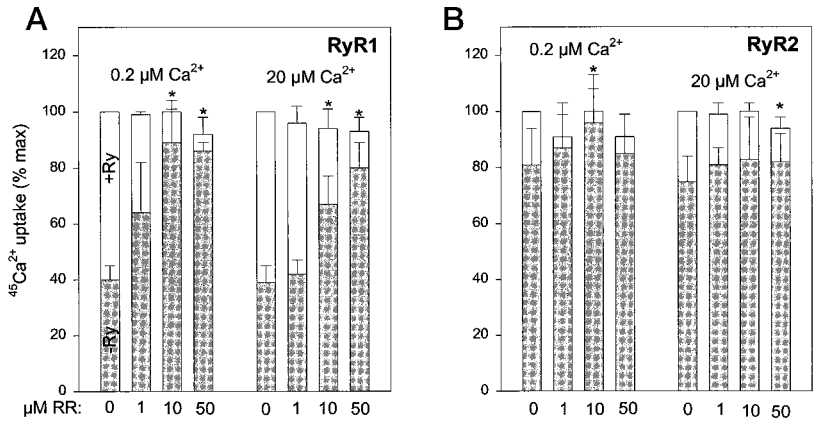

FIG. 2. **Comparison of effects of RR on $^{45}Ca^{2+}$ uptake by skeletal and cardiac muscle SR vesicles.** ATP-dependent $^{45}Ca^{2+}$ uptake by ryanodine-treated and -untreated RyR1 and RyR2 SR vesicles was determined as in Fig. 1. Vesicles were incubated for 2 min in $^{45}Ca^{2+}$ uptake medium containing the indicated RR and free Ca^{2+} concentrations. The maximum values (100% = maximum value of ryanodine-treated vesicles in the absence of RR) corresponded to 63 ± 17 and 138 ± 19 nmol of $^{45}Ca^{2+}$/mg of protein for skeletal muscle SR vesicles and 11 ± 4 and 34 ± 7 nmol of $^{45}Ca^{2+}$/mg of protein for cardiac muscle SR vesicles at 0.2 and 20 μM Ca^{2+}, respectively. Data are the mean ± S.E. of three or four experiments. *, $p < 0.05$ as determined by Student's paired *t* test.

ryanodine was used to obtain information on the mechanism of RR inhibition of RyR1 and RyR2 independent of SR Ca^{2+} pump activity. [^{3}H]Ryanodine binding is widely used as a probe of channel activity because of its preferential binding to open RyR ion channel states (1–5). Fig. 3 compares the Ca^{2+} dependence of [^{3}H]ryanodine binding to skeletal and cardiac muscle SR vesicles in 0.25 M KCl solutions containing varying concentrations of RR. In the absence of RR, two bell-shaped activation/inactivation curves were obtained. In agreement with previous reports (1–5), the binding data indicate that RyR1 and RyR2 are activated by Ca^{2+} binding to cytosolic high affinity receptor sites and inhibited by Ca^{2+} binding to low affinity sites, with higher Ca^{2+} concentrations required to inhibit RyR2. Higher RR concentrations were required to inhibit [^{3}H]ryanodine binding to RyR2 than RyR1 (Fig. 3). RR decreased the amounts of [^{3}H]ryanodine bound without markedly changing the Ca^{2+} dependence of [^{3}H]ryanodine binding.

The effects of RR concentration on [^{3}H]ryanodine binding were determined at 2.5, 15, and 200 μM Ca^{2+} and at 15 μM free Ca^{2+} in the presence of the nonhydrolyzable ATP analog AMPPCP. We also tested conditions comparable to those in Figs. 1 and 2 by using solutions that contained 5 mM MgAMPPCP and 20 μM or 200 μM free Ca^{2+}. In the absence of RR, the highest binding of [^{3}H]ryanodine to RyR1 was observed at 15 μM free Ca^{2+} and 5 mM AMPPCP (Fig. 4*A*) and to RyR2 at 200 μM Ca^{2+} (Fig. 4*B*). The results agree with single channel measurements that μM Ca^{2+} and mM ATP optimally activate RyR1, whereas RyR2 is nearly fully activated by μM Ca^{2+} alone (see Figs. 6*C* and 9*A*). RR inhibited [^{3}H]ryanodine binding to RyR1 and RyR2 in a concentration-dependent manner (Fig. 4). Solid lines in Fig. 4 were obtained by fitting the [^{3}H]ryanodine binding data to Equation 1. The average Hill inhibition constants (K_i) and coefficients (n_i) (Table I) indicate that RR was more effective in inhibiting [^{3}H]ryanodine binding at 2.5 μM Ca^{2+} than at 15 μM or 200 μM Ca^{2+}. The binding data could not be fitted when it was assumed that RR inhibited [^{3}H]ryanodine binding by competing with Ca^{2+} for the Ca^{2+} activation sites via a competitive mechanism (not shown). RR was least effective in inhibiting the RyRs in 15 μM Ca^{2+} medium containing 5 mM AMPPCP (Fig. 4 and Table I). Similarly, the presence of 5 mM MgAMPPCP decreased the effectiveness of RR in inhibiting [^{3}H]ryanodine binding to RyR1 and RyR2. Scatchard analysis of two sets of binding data from Fig. 4 indicated that RR inhibited [^{3}H]ryanodine binding by decreasing the B_{max} and K_D values (Fig. 5). Taken together, the [^{3}H]ryanodine binding data suggest that RR inhibits RyR1 and RyR2 by noncompetitive interactions between RyR Ca^{2+} regulatory and RR inhibition sites.

RR Inhibits and Induces Subconductances in Single RyR1s—The kinetics of RR inhibition of the RyRs were further examined in single channel measurements. Proteoliposomes containing purified RyR were fused with planar lipid bilayers. A strong dependence of single channel activities on *cis*-Ca^{2+} concentration indicated that the large cytosolic region of the channels faced the *cis* (cytosolic) chamber in a majority (>98%) of the recordings (34, 35). Channels that could not be activated by

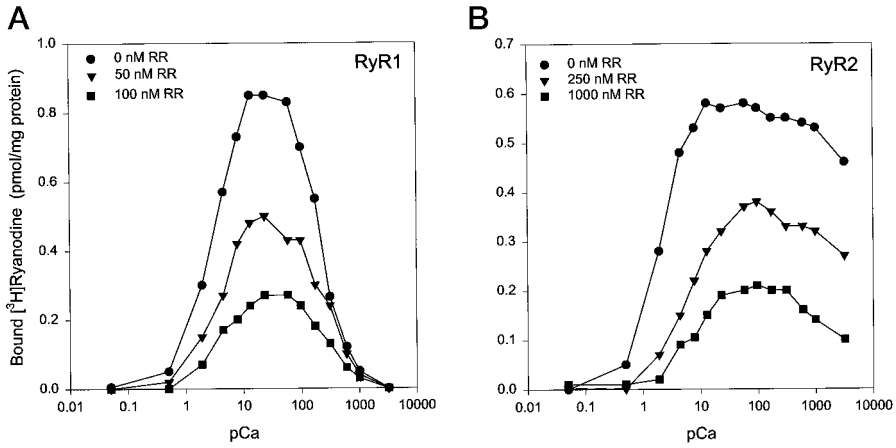

FIG. 3. **Effects of RR on Ca^{2+} activation/inactivation profiles of [^{3}H]ryanodine binding to skeletal muscle (*A*) and cardiac muscle (*B*) SR vesicles.** Specific [^{3}H]ryanodine binding was determined as described under "Experimental Procedures" in 0.25 M KCl medium containing 1 nM [^{3}H]ryanodine, the indicated concentrations of RR, and free Ca^{2+}. One of two similar experiments is shown.

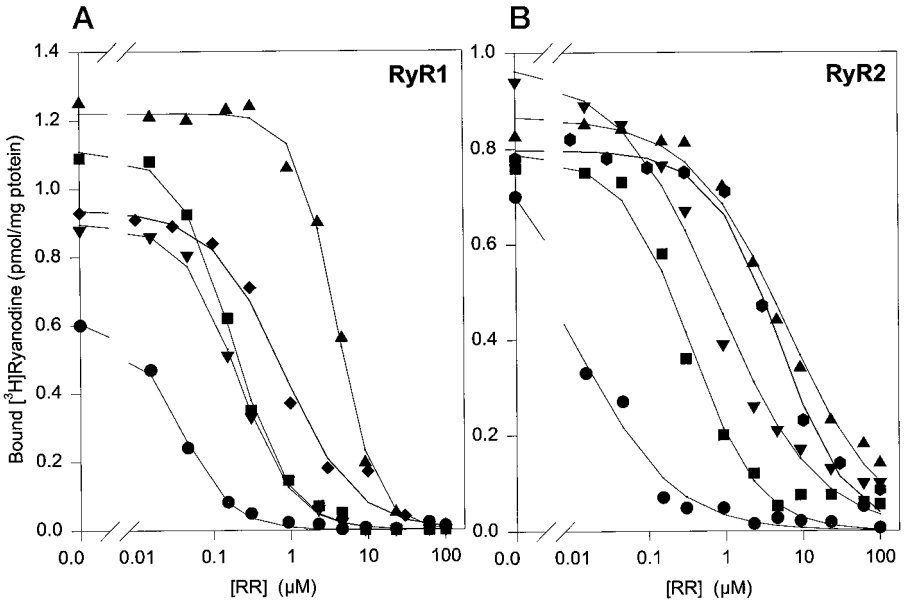

FIG. 4. **Effects of RR concentration on [^{3}H]ryanodine binding to skeletal muscle (*A*) and cardiac muscle (*B*) SR vesicles.** Specific [^{3}H]ryanodine binding was determined as described under "Experimental Procedures" in 0.25 M KCl medium containing the indicated concentrations of RR, 2.5 μM free Ca^{2+} (●), 15 μM free Ca^{2+} in the absence (■) and presence (▲) of 5 mM AMPPCP, 20 μM free Ca^{2+} in the presence of 5 mM MgAMPPCP (*A,* ♦), or 200 μM free Ca^{2+} in the absence (▼) and presence (B, *filled hexagon*) of 5 mM MgAMPPCP. Binding data were fitted by Equation 1 (*lines*). Average Hill inhibition constants and coefficients of several experiments are shown in Table I.

TABLE I

Effects of RR on [^{3}H]ryanodine binding to RyR1 and RyR2

Hill inhibition constants (K_i) and coefficients (n_i) were obtained as indicated in the legend to Fig. 4. Values are the mean ± S.E. of the number of experiments shown in parentheses.

Condition	RyR1		RyR2	
	K_i	n_i	K_i	n_i
	nM		*nM*	
2.5 μM Ca^{2+}	49 ± 16 (3)	1.5 ± 0.3 (3)	16 ± 2 (3)	1.0 ± 0.1 (3)
15 μM Ca^{2+}	91 ± 44 (5)	1.3 ± 0.2 (5)	156 ± 103 (6)	1.1 ± 0.2 (6)
200 μM Ca^{2+}	109 ± 49 (5)	1.3 ± 0.2 (5)	434 ± 187 (8)	1.1 ± 0.3 (8)
15 μM Ca^{2+} + 5 mM AMPPCP	2970 ± 1620 (3)	1.5 ± 0.2 (3)	5920 ± 390 (3)	0.7 ± 0.1 (3)
20 μM Ca^{2+} + 5 mM MgAMPPCP	660 ± 240 (3)	1.1 ± 0.2 (3)	3420 ± 1000 (3)	1.0 ± 0.2 (3)
200 μM Ca^{2+} + 5 mM MgAMPPCP	—[a]	—	4150 ± 1300 (3)	0.9 ± 0.2 (3)

[a] —, not determined.

1–10 μM Ca^{2+} were discarded. The majority of channels were recorded in symmetric 0.25 M KCl solutions rather than with a lumenal Ca^{2+} solution to eliminate large Ca^{2+} gradients near the cytosolic channel pore sites (34). With K^+ as the current carrier, single channel conductance was ~790 pS (30).

Fig. 6*A* shows six current traces of two RyR1 ion channels. In the *top traces* (control), channels were recorded in the presence of 20 μM cytosolic Ca^{2+} and 3–4 μM (contaminant) lumenal Ca^{2+} at holding potentials of −40 mV (*left panel*) and +40 mV (*right panel*). The addition of 10 and 25 nM cytosolic RR induced prolonged channel closings and decreased P_o to close to 0 at 25 nM RR. No subconductances were observed before and after the addition of RR. Equation 2 provided a good fit to the single channel data for RyR1s recorded at both holding potentials (n = 5–6; data not shown). An average Hill inhibition constant of approximately 5 nM (Table II) compared with 90 nM (Table I) suggests that RR was more effective in inhibiting the skeletal channel in the single channel than [^{3}H]ryanodine binding experiments. Average Hill coefficients of 1.3–1.6 (Table II) suggest that RR inhibited single RyRs through a weak cooperative interaction.

RR was similarly effective in inhibiting single RyR1s recorded at 200 μM rather than 20 μM free cytosolic Ca^{2+} (Fig. 6*B* and Table II). Again, no subconductances were evident before or after the addition of RR. A single skeletal muscle channel recorded in the presence of 20 μM free cytosolic Ca^{2+} and 2 mM

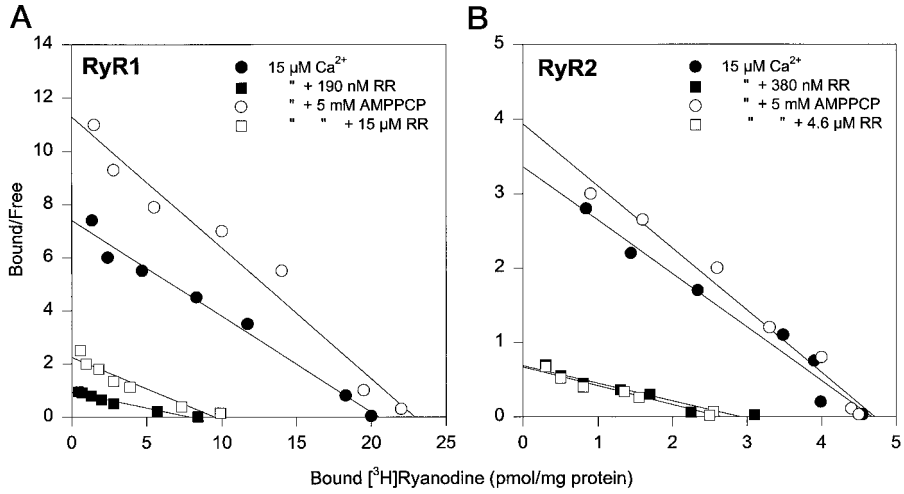

FIG. 5. **Scatchard analysis of [^{3}H]ryanodine binding to skeletal muscle (*A*) and cardiac muscle (*B*) SR vesicles in the presence and absence of RR.** Specific [^{3}H]ryanodine binding was determined as described under "Experimental Procedures" in 0.25 M KCl medium containing 0.5–50 nM [^{3}H]ryanodine and the indicated concentrations of RR, AMPPCP, and free Ca^{2+}.

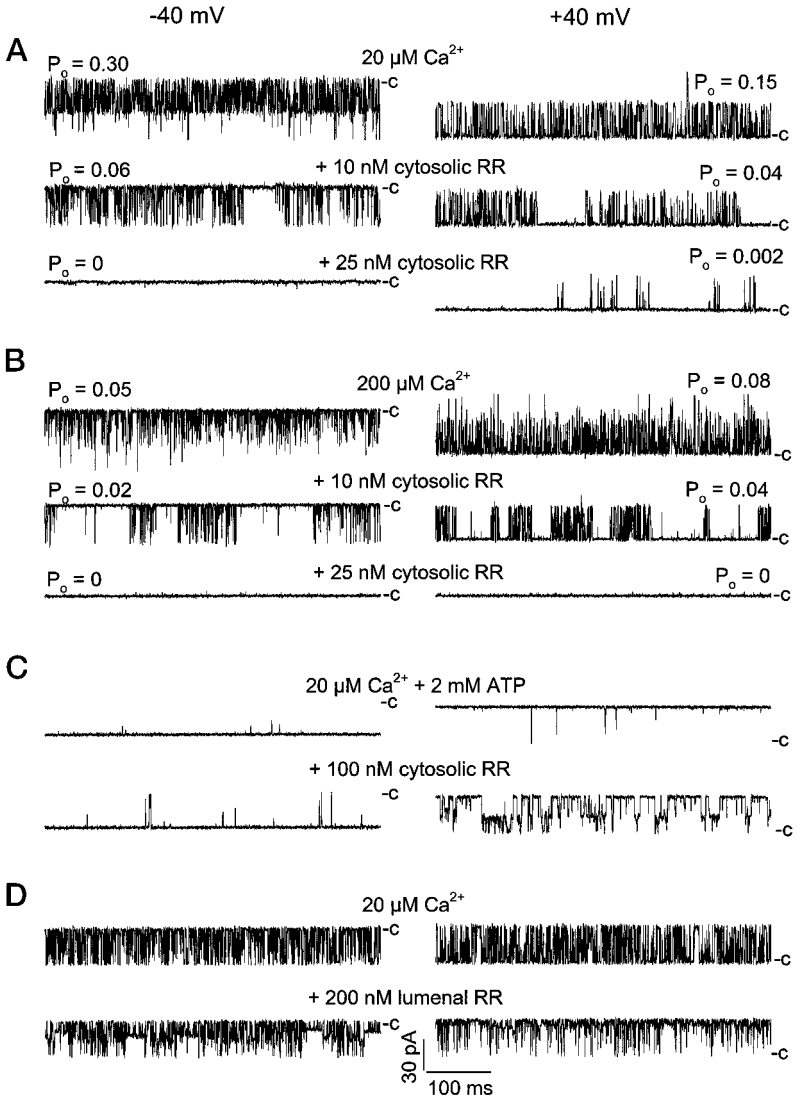

FIG. 6. **Effects of cytosolic and lumenal RR on single RyR1s.** Single channel currents were recorded at −40 mV (*left panels,* downward deflections from closed levels, *c*) and +40 mV (*right panels,* upward deflections) in symmetric 0.25 M KCl, 10 mM KHepes, pH 7.4, medium containing the indicated concentrations of free cytosolic Ca^{2+} and ATP before (*A–D, top traces*) and after the addition of the indicated concentrations of cytosolic or lumenal RR. Lumenal (contaminant) Ca^{2+} was ~4 μM. *A* and *B,* effect of cytosolic RR on channel activity of two RyR1s at 20 μM (*A*) and 200 μM (*B*) free Ca^{2+}. *C,* effect of cytosolic RR on channel activity of single RyR1 at 20 μM free Ca^{2+} and 2 mM ATP. RR induced four substates with conductances of 12.5, 28, 45, and 60% of the control conductance in a voltage-dependent manner. The substate with a conductance of 45% of the control was the predominant one. *D,* effect of lumenal RR on channel activity of single RyR1 at 20 μM free cytosolic Ca^{2+}. Lumenal RR induced three voltage-dependent substates with conductances of 85, 55, and 25% of the control conductance.

ATP was nearly fully activated in the absence of RR (Fig. 6*C*). The addition of 100 nM cytosolic RR resulted in several subconductances at +40 mV but not −40 mV. The predominant subconductance corresponded to 45% of the full conductance at +40 mV and was interrupted by frequent transitions to a closed state. The presence of lumenal RR induced three predominant subconductances, corresponding to 85, 55, and 25% of the full conductance (Fig. 6*D*). The three subconductances were observed at both −40 mV and +40 mV, with the frequency of substate formation being higher at the negative holding potential ($n = 3$).

The data shown in Fig. 6, *C* and *D,* indicate that formation of subconductances depended on membrane potential. Cytosolic RR-related subconductances were observed at positive membrane potentials that favored cytosolic to lumenal cation fluxes. In the presence of lumenal RR, subconductances were prefer-

TABLE II
Effects of RR on single channel properties of RyR1 and RyR2
Single channel parameters were obtained as described in the text. Values are the means ± S.E. of number of experiments in parentheses.

Condition	RyR1		RyR2	
	Cytosol → Lumen (H.P. >0)[a]	Lumen → Cytosol (H.P. <0)	Cytosol → Lumen (H.P. >0)	Lumen → Cytosol (H.P. <0)
10 μM Ca^{2+}, cytosolic RR				
P_o: K_i (nM)	5.6 ± 2.3 (5)	4.9 ± 3.0 (5)	46 ± 1 (6)	43 ± 9 (6)
n_i	1.3 ± 0.6 (5)	1.6 ± 0.2 (5)	2.4 ± 0.4 (6)	2.3 ± 0.4 (6)
200 μM Ca^{2+}, cytosolic RR				
P_o: K_i (nM)	4.4 ± 1.8 (3)	4.1 ± 2.0 (3)	—	387 ± 45 (5)
n_i	1.2 ± 0.4 (3)	1.1 ± 0.3 (3)	—	2.1 ± 0.5 (5)
P_{sub}/P_{tot}: K_a (nM)	N.D.	N.D.	140 ± 20 (5)	N.D.
n_a			1.6 ± 0.1 (5)	
Z_{tot}			1.3 ± 0.1 (9)	
10 μM Ca^{2+}, lumenal RR				
P_o: K_i (nM)	—	—	>1000	—
n_i			—	—
P_{sub}/P_{tot}: K_a (nM)	—	—	N.D.	1700 ± 700 (4)
n_a				1.7 ± 0.3 (4)
Z_{tot}				0.8 ± 0.1 (4)

[a] H.P., holding potential; N.D., not detected; —, not determined.

entially formed at negative membrane potentials that favored lumenal to cytosolic cation fluxes. The results raised the possibility that highly positively charged RR molecules enter the conductance pathway of RyR1, resulting in reduction of single channel currents.

The SR membrane is highly permeable to monovalent cations and anions, which suggests that the membrane potential across the SR in resting muscle is likely close to 0 mV (36). The effects of cytosolic and lumenal RR on single RyR1s were therefore also determined at 0 mV holding potential in a symmetric 0.25 M KCl solution with 10 mM lumenal Ca^{2+}, with Ca^{2+} being the conducting ion. In this condition, a Ca^{2+} current could be measured, ranging from 2 pA (Fig. 7*C*) to 3.1 pA (Fig. 7, *A* and *B*). In Fig. 7, *A* and *B,* single RyR1 channels were initially recorded under conditions similar to those in Fig. 6*C, i.e.* in the presence of 20 μM free cytosolic Ca^{2+} and 2 mM ATP. Both channels were nearly fully activated in the absence of RR (*top traces*). Addition of 250 nM cytosolic RR induced channel closings and a subconductance ($P_{sub} \sim 0.1$) corresponding to ~50% of the full conductance (Fig. 7*A*). In Fig. 7*B,* the presence of 300 nM lumenal RR induced, similar to the result shown in Fig. 6*D,* multiple subconductances corresponding to ~25, 60, and 75% of the full conductance. In Fig. 7*C,* a single RyR1 channel was nearly fully activated using conditions closely matching those in Figs. 1 and 4, *i.e.* 20 μM free cytosolic Ca^{2+} and 5 mM MgATP. The addition of 60 nM cytosolic RR induced an infrequent subconductance ($P_{sub} \sim 0.02$) corresponding to ~25% of the full conductance. RR concentrations greater than those shown in Fig. 7 resulted in complete channel closings in a majority of the single channel recordings. Taken together, the data shown in Fig. 7 show that RR induces subconductances in Ca^{2+}-conducting RyR1 recorded at a membrane potential considered to be physiologically relevant.

RR Inhibits and Induces Subconductances in Single RyR2s—A more detailed kinetic analysis of the effects of RR on single RyR ion channels was carried out using RyR2. Six current traces of a single K^+ conducting cardiac release channel are shown in Fig. 8. In the *top traces* (control), the channel was recorded in the presence of 10 μM cytosolic Ca^{2+} and 3–4 μM lumenal Ca^{2+} at holding potentials of −30 mV (*left panel*) and +30 mV (*right panel*). The addition of 30 and 60 nM cytosolic RR decreased channel activity at both holding potentials by greater than 50 and 90%, respectively. As observed for RyR1 (Fig. 6*A*), RR formed long channel closings without inducing subconductances. Hill inhibition constants of 46 ± 1 nM at +30 mV and 43 ± 9 nM at −30 mV ($n = 6$) indicated a voltage-independent inhibition of channel activity (Table II). Hill inhibition coefficients of 2.4 ± 0.4 and 2.3 ± 0.4 suggested that more than one RR molecule was involved in inhibiting channel activity. Kinetic analysis showed that the addition of 60 nM cytosolic RR decreased the number of channel events/min from 19256 ± 5339 to 7641 ± 2252 and the mean open time from 6.6 ± 1.4 to 3.5 ± 1.6 ms ($n = 10$). The mean closed time increased from 3.0 ± 0.7 to 39.2 ± 13.7 ms. Thus, a major effect of cytosolic RR

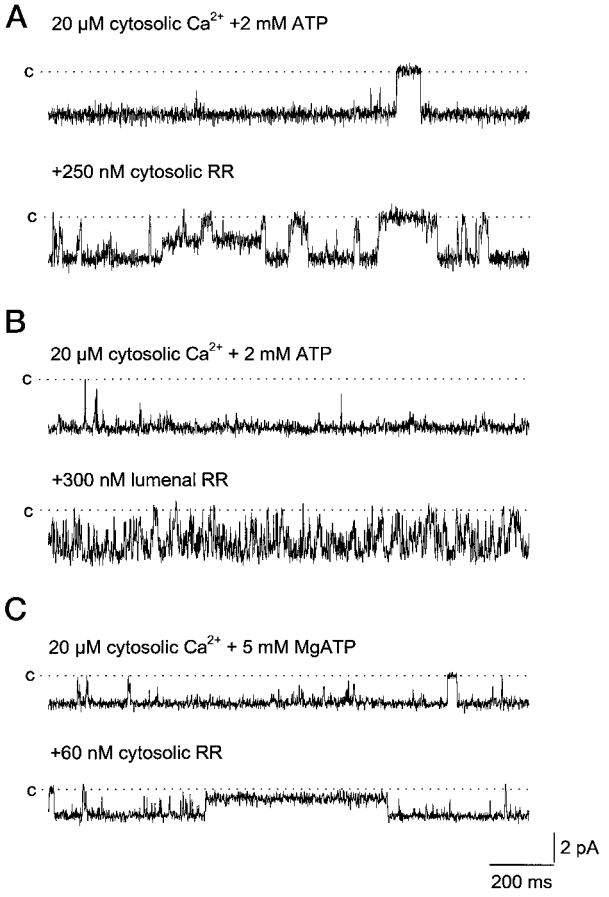

FIG. 7. **Effects of RR on Ca^{2+}-conducting RyR1 at 0 mV.** Single channel currents were recorded at 0 mV (downward deflections from closed levels, *c* and *dotted lines*) in symmetric 0.25 M KCl, pH 7.4, solutions containing 10 mM lumenal Ca^{2+} and the indicated cytosolic Ca^{2+}, Mg^{2+}, and ATP concentrations and cytosolic (*A* and *C*) or lumenal (*B*) RR concentration. Each panel shows one of three or four similar recordings. Single channel currents were filtered at 300 Hz to decrease noise.

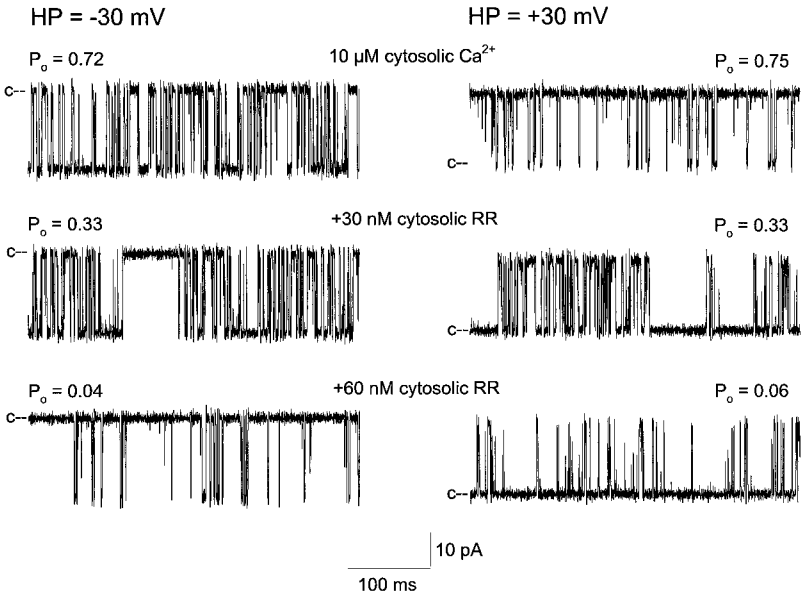

FIG. 8. **Inhibition of RyR2 by cytosolic RR at 10 μM cytosolic Ca^{2+}.** Single channel currents were recorded at −30 mV (*left panels,* downward deflections) and +30 mV (*right panels,* upward deflections) in symmetrical 0.25 M KCl, 20 mM KHepes, pH 7.4, medium containing 10 μM cytosolic Ca^{2+}, contaminant (~4 μM) lumenal Ca^{2+}, and 0 (*top traces*), 30 (*middle traces*), or 60 (*bottom traces*) nM cytosolic RR. Average Hill inhibition constants and coefficients of several experiments are shown in Table II.

was to increase the duration of the closed events.

The effects of cytosolic RR on RyR2 were also evaluated at a cytosolic [Ca^{2+}] of 200 μM. At this Ca^{2+} concentration the cardiac channel is close to maximally activated (Fig. 9*A, top panels*). Addition of 60, 150, and 220 nM cytosolic RR induced a subconductance state at +30 mV but not at −30 mV. The current amplitude histogram of Fig. 9*B* shows that the frequency but not current amplitude of the substate depended on RR concentration. The histogram shows open channel currents of ~24 pA. The addition of RR resulted in a major substate with a current of 8–9 pA at +30 mV and closed channel events (at 0 pA) at −30 and +30 mV. Current-voltage relationships of the full and subconductance states in the absence and presence of 150 nM RR are shown in Fig. 9*C*. RR did not affect the full open conductance at negative and positive holding potentials. In contrast, the subconductance current-voltage relationship was nonlinear, with the subconductance corresponding to 28 ± 5 and 12 ± 2% of the full conductance at +30 mV and +60 mV, respectively ($n = 5$). A decrease to 60 nM RR or increase to 220 nM RR (Fig. 9*A*) was without effect on the current-voltage relationship of the subconductance (not shown). The fractional increase in channel open probability of the substate (P_{sub}/P_{tot}) at +30 mV (Fig. 9*A*) could be fitted by Equation 3, which describes the $O_{Ca} \Leftrightarrow O_{sub}$ transitions (Fig. 9*D, solid line*). The average Hill constant was 140 ± 20 nM (Table II). A Hill coefficient of 1.6 ± 0.1 suggested that more than one RR molecule was involved in forming the substate. RR also increased the rate of full channel closings (Fig. 9*A*). This effect was analyzed in single channel recordings obtained at negative holding potentials because these lacked subconductances, therefore simplifying the analysis. *Broken lines* in Fig. 9*D* were obtained by fitting P_o to Equation 2. The average Hill constants of the full channel closings were 2–3-fold higher than the Hill constants of substate formation and ~10-fold higher than the Hill inhibition constants at 10 μM Ca^{2+} (Table II).

RR formed a subconductance in 8 out of 10 recordings at 200 μM Ca^{2+} and 1 out of 2 recordings at 5 mM Ca^{2+}. In the remaining three recordings, RR decreased channel activity without inducing a subconductance state. Time analysis of channel recordings at 200 μM Ca^{2+} suggested differences in channel gating that appeared to be directly related to the ability of channels to form subconductances. Channels that formed subconductances gated more slowly before the addition of RR than channels that did not form subconductances (mean open time, 32 ± 9 ms ($n = 8$) *versus* 3 ms ($n = 2$), respectively). This result suggests that slowly gating channels are more likely to form subconductances than rapidly gating channels. In support of this idea, we found that subconductances were formed at positive membrane potentials when RyR2 was recorded in the presence of 10 μM cytosolic free Ca^{2+}, 5 mM ATP, and 300 nM RR (not shown). This condition in the absence of RR resulted in a nearly fully activated channel with long open times.

Lumenal RR induced a major subconductance in RyR2 at negative membrane potentials (Fig. 10). A single Ca^{2+}-activated RyR2 was recorded at −30 mV and +30 mV in the presence of 10 μM cytosolic Ca^{2+} and increasing concentrations of lumenal RR. In the absence of RR (Fig. 10*A, top traces*), the channel was nearly fully activated. Addition of 150–500 nM lumenal RR affected the channel (Fig. 10*A*) in a manner reminiscent of that of cytosolic RR in the presence of 200 μM Ca^{2+} (Fig. 9*A*), except that lumenal RR induced a major substate at the negative (Fig. 10*A, left panel*) instead of positive (*right panel*) holding potential. Fig. 10*B* shows IV curves of the full and subconductance states in the presence and absence of 150 nM lumenal RR. The presence of RR did not affect the full open conductance, whereas the lumenal RR-related subconductance current showed a slightly rectifying behavior with a conductance corresponding to 49 ± 1 and 40 ± 1% of the full conductance at −30 and −60 mV, respectively (Fig. 10*B*, $n = 5$). An increase in cytosolic Ca^{2+} from 10 to 200 μM and a change in lumenal RR concentration were without effect on the current-voltage relationship of the subconductance (not shown).

Lumenal RR induced a major subconductance with a lower affinity than cytosolic RR, as indicated by a Hill constant of 1700 ± 700 nM for lumenal RR (Fig. 10*C* and Table II) as compared with 140 ± 20 nM for cytosolic RR (Fig. 9*D* and Table II). At +30 mV in the presence of 300 and 500 nM RR, brief, poorly resolved channel closings were observed (Fig. 10*A*). Their occurrence suggested that RR also affected the channel at positive holding potentials, but unlike at −30 mV, the durations were too short to be fully resolved at the limited time resolution of the bilayer set-up (35). In addition, small, variable increases in full channel closings were observed at elevated lumenal RR (Fig. 10*C* and Table II).

Cytosolic RR was effective in inducing a subconductance at positive holding potentials (Fig. 9), whereas lumenal RR was effective at negative potentials (Fig. 10). The voltage depend-

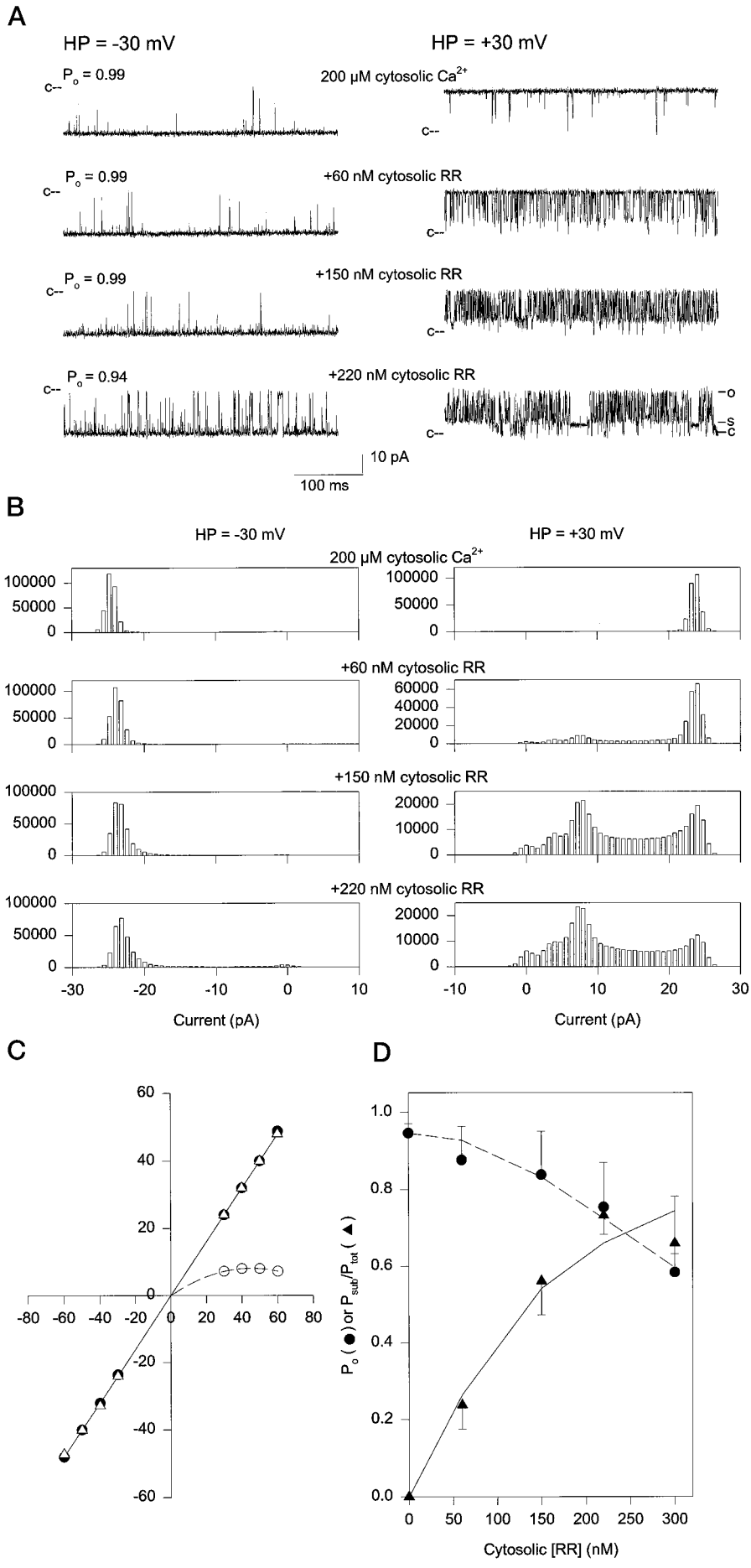

FIG. 9. **Effects of cytosolic RR on single cardiac channel recorded at 200 μM cytosolic Ca^{2+}.** *A,* single channel currents were recorded as in Fig. 8 except that the cytosolic [Ca^{2+}] was 200 μM. An RR-related subconductance state was evident at the positive but not negative holding potential. *B,* current amplitude histograms at −30 mV and +30 mV and 0, 60, 150, and 220 nM cytosolic RR. The occurrence but not the current amplitude (8–9 pA at +30 mV) of the subconductance increased with RR concentration. *C,* current and voltage relationships of full conductance state in the absence of RR (●) and full conductance (△) and subconductance (○) states in the presence of 60 nM cytosolic RR. Values are means ± S.E. of five experiments. (Error bars (not shown) were smaller than the symbols.) *D,* dependence of P_{sub}/P_{tot} (▲) (at +30 mV) and P_o (●) (at −30 mV) on cytosolic RR concentration. *Solid* and *broken lines* were calculated according to Equations 3 and 2, respectively. Data are the means ± S.E. of five experiments. Average Hill inhibition constants and coefficients are shown in Table II.

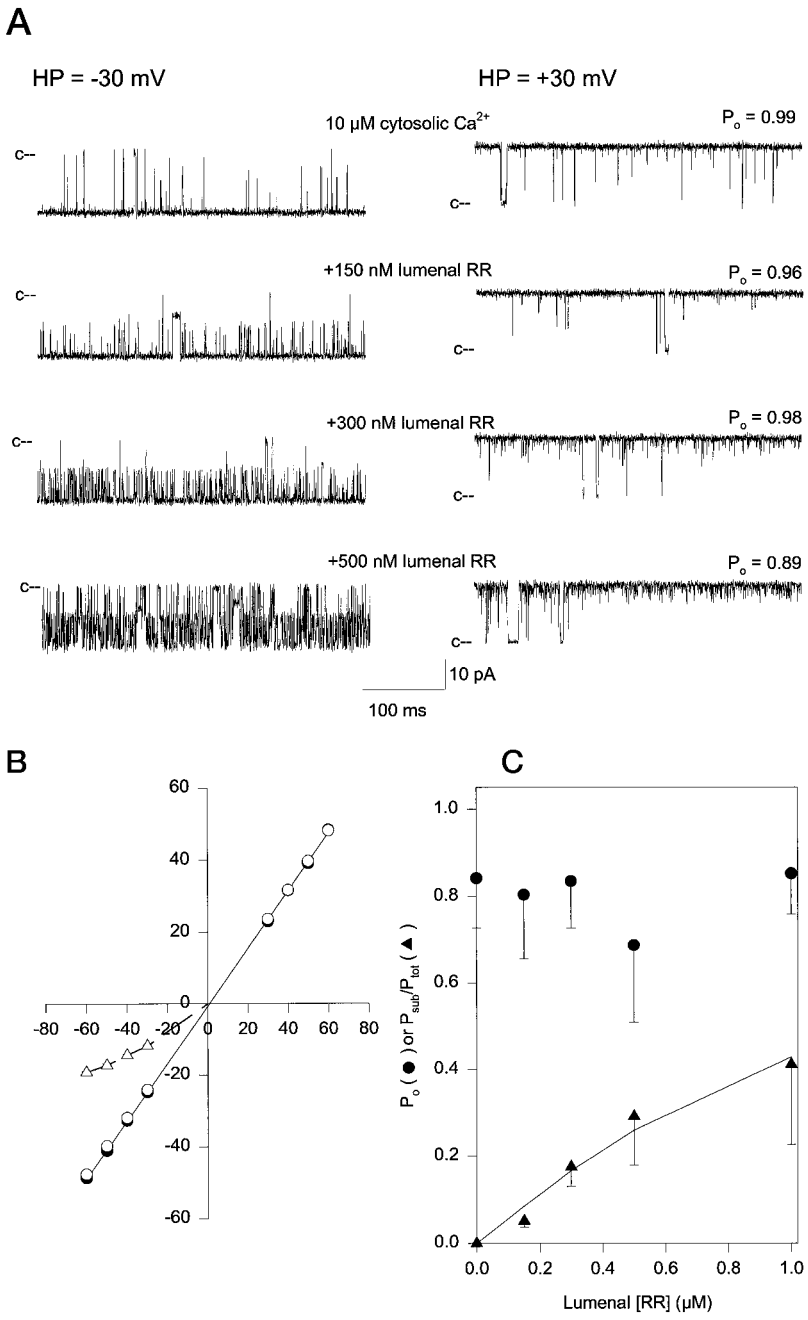

FIG. 10. **Effects of lumenal RR on single RyR2.** *A,* a single cardiac channel was recorded as in Fig. 8 except that increasing RR concentrations were added to the lumenal instead of the cytosolic chamber of the bilayer apparatus. At negative holding potential a lumenal RR-related subconductance state (see *left panels*) became increasingly obvious as the RR concentration was increased, but the current of the subconductance did not change with RR concentrations. *B,* current-voltage relationships of full conductance state in the absence of RR (●) and full conductance (○) and subconductance (△) states in the presence of 150 nM lumenal RR. Values are means ± S.E. of five recordings (error bars are smaller than symbols). *C,* dependence of P_o (●) (at +30 mV) and P_{sub}/P_{tot} (▲) (at −30 mV) on lumenal RR concentration. *Solid line* was calculated according to Equation 3. Data are the means ± S.E. of four experiments. Average Hill constants and coefficients are shown in Table II.

ence of P_{sub}/P_{full} on holding potential was analyzed by the Boltzmann equation given under "Experimental Procedures" (Equation 4). A single RyR2 was recorded in the presence of 200 μM cytosolic Ca^{2+} and 60, 150, and 220 nM cytosolic RR. Three lines with similar slopes but different intercepts were obtained at the three RR concentrations (Fig. 11). The mean slope was 0.050 ± 0.002, from which an effective gating charge (Z_{tot}) of 1.3 ± 0.1 was obtained (Table II). P_{sub}/P_{full} of the lumenal RR-related substate of RyR2 obeyed Equation 4, with a Z_{tot} value of 0.8 ± 0.1 (Table II).

In Fig. 12, the effects of cytosolic and lumenal RR on single RyR2 channels were determined as in Fig. 7, *i.e.* at 0 mV with 10 mM lumenal Ca^{2+} as the current carrier. Single channel conductance varied from 2 pA (Fig. 12*D*) to 3.4 pA (Fig. 12*A*). In Fig. 12, *A* and *B,* single RyR2 channels were recorded under conditions similar to those in Figs. 9 and 10, *i.e.* in the presence of 200 and 10 μM free cytosolic Ca^{2+}, respectively. Addition of 300 nM cytosolic (Fig. 12*A*) and 500 nM lumenal (Fig. 12*B*) RR induced subconductances (P_{sub} <0.06) corresponding to ~25 and 35% of the full conductance, respectively. In Fig. 12, *C* and *D,* single RyR2 channels were recorded in the presence of 5 mM cytosolic MgATP and 20 or 200 μM free Ca^{2+}, *i.e.* under conditions similar to those in Figs. 2 and 4. In the presence of cytosolic RR, subconductances were observed in the 200 μM Ca^{2+} medium (Fig. 12*D,* P_{sub} ~0.01) but rarely in the 20 μM (Fig. 12*C,* $P_{sub} < 0.001$) Ca^{2+} medium. RR concentrations in excess of those in Fig. 12 resulted in complete channel closings. We conclude from these observations that RR induces subconductances in Ca^{2+}-conducting RyR2 channels recorded at 0 mV.

DISCUSSION

In the present study, the effects of RR on the cardiac and skeletal muscle RyRs were investigated in vesicle Ca^{2+} flux, [^{3}H]ryanodine binding, and single channel measurements. Scheme 1 describes the results.

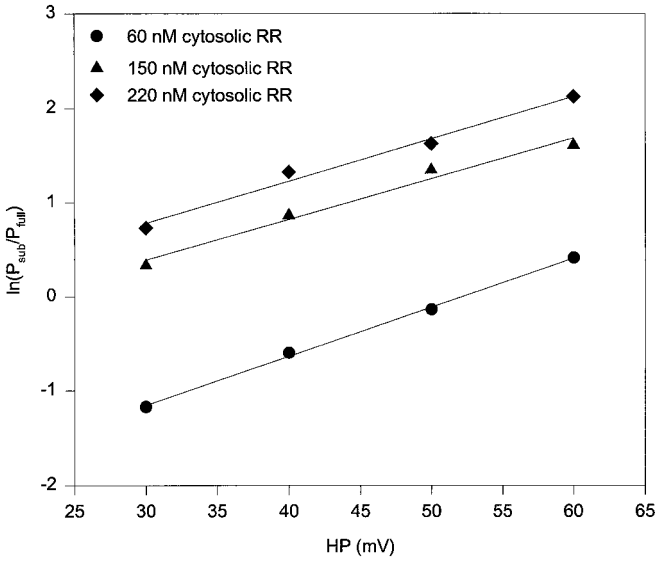

FIG. 11. **Voltage dependence of cytosolic RR-related subconductance.** Voltage dependence of P_{sub}/P_{full} of a single RyR2 ion channel (Fig. 9A) was determined according to Equation 4. Linear correlation coefficients were 1.0 (●) (60 nM RR), 0.99 (▲) (150 nM RR), and 0.99 (◆) (220 nM RR). Average Z_{tot} values of several experiments are shown in Table II.

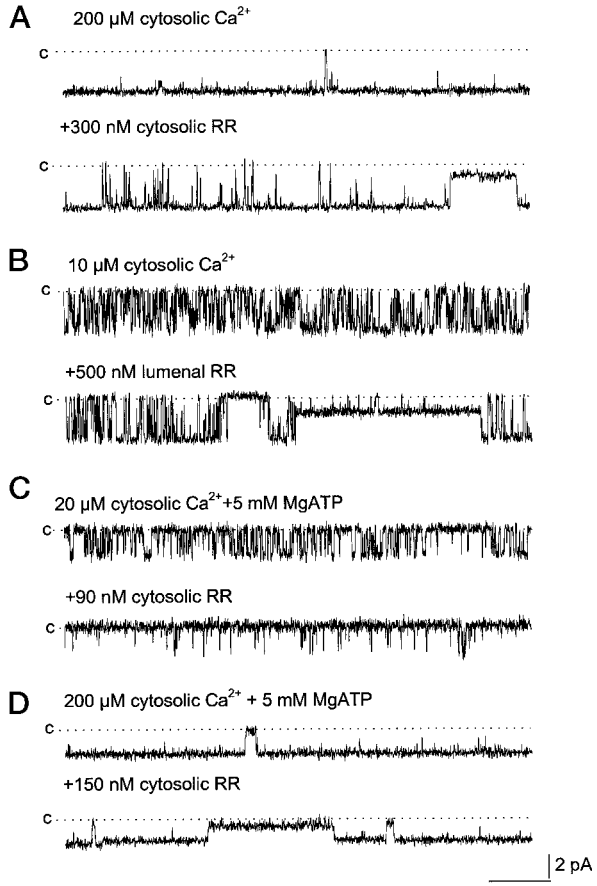

FIG. 12. **Effects of RR on Ca^{2+}-conducting RyR2 at 0 mV.** Single channel currents were recorded at 0 mV (downward deflections from closed levels, *c* and *dotted lines*) in symmetric 0.25 M KCl, pH 7.4, solutions containing 10 mM lumenal Ca^{2+} and the indicated cytosolic Ca^{2+}, Mg^{2+}, and ATP concentrations and cytosolic (*A, C,* and *D*) or lumenal (*B*) RR concentration. Each panel shows one of two to five similar recordings. Frequency, 300–500 Hz.

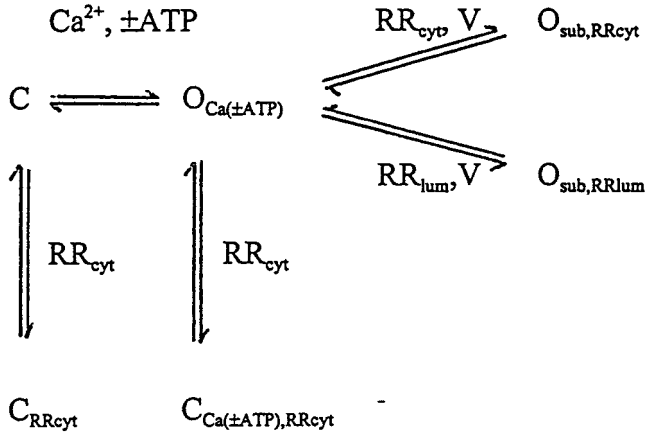

SCHEME 1

It is assumed that RR binds to voltage-independent and -dependent sites of the RyRs. The Ca^{2+} release channels are present in a closed Ca^{2+}-free form (C) at cytosolic [Ca^{2+}] <0.1 μM and Ca^{2+}-activated form ($O_{Ca(-ATP)}$) at cytosolic [Ca^{2+}] >0.1 μM. Micromolar cytosolic Ca^{2+} and the presence of millimolar ATP ($\pm Mg^{2+}$) yields $O_{Ca(\pm ATP)}$. Binding of RR to cytosolic channel sites of C and $O_{Ca(\pm ATP)}$ results in closed channel states C_{RRcyt} and $C_{Ca(\pm ATP),RRcyt}$. Cytosolic and lumenal RR binding to sites of the open channels is influenced by membrane potential and results in subconductance channel states, $O_{sub,RRcyt}$ and $O_{sub,RRlum}$, respectively. The oligomeric RyR contains cooperatively interacting Ca^{2+} activation and RR binding sites; however, only one each is shown. Also not shown are the channel Ca^{2+}-inactivation sites and channel closings originating from substates.

Vesicle-Ca^{2+} flux measurements suggest the effectiveness of RR in inhibiting RyRs depended on Ca^{2+} concentration. One likely reason for the requirement of relatively high RR concentrations in these studies was that Ca^{2+} flux measurements were carried out in the presence of the allosteric activator molecule ATP (5). This notion was confirmed by our [^{3}H]ryanodine binding experiments that showed that the presence of AMPPCP and MgAMPPCP reduced RR inhibition of RyR. In overlay studies with RyR1 fusion peptides, RR bound to several Ca^{2+} binding peptides (37), raising the possibility that RR competes with Ca^{2+} for the Ca^{2+} activation sites. In support of this suggestion, RR decreased [^{3}H]ryanodine binding by competitive inhibition (18). Alternatively, AMPPCP might have induced a conformational change that lowers the affinity of RR binding to sites not directly involved in regulation by Ca^{2+}. In support of a noncompetitive mechanism is the finding that RR decreased B_{max} and increased K_D of [^{3}H]ryanodine binding (Ref. 16 and this study), with the latter effect being due to a slower association rate (16). In single channel experiments at low micromolar [Ca^{2+}] in the absence of ATP, cytosolic RR decreased the channel activities to the same extent at negative and positive holding potentials, without the appearance of channel states of reduced conductance. At elevated Ca^{2+} concentrations, cytosolic RR also induced full channel closings at both holding potentials. These were analyzed for RyR2 only at negative holding potentials, at which substates were not observed. Because RR is a polycationic molecule, a voltage-independent inhibition suggests that RR fully closed the channels by binding to cytosolic sites that are located outside the electrical field.

Several differences were observed in the interaction between RR and the RyRs. At 10–15 μM Ca^{2+}, RR was more effective in inhibiting the cardiac and skeletal RyRs in single channel than [^{3}H]ryanodine binding measurements. An approximately 3- and 20-fold difference was observed in the K_i values for the

cardiac and skeletal muscle RyRs, respectively. For RyR1, average Hill inhibition coefficients of 1.1–1.6 were obtained, suggesting no or a weak cooperative binding of RR. Hill inhibition coefficients of 2.4 and 2.3 suggest that RR inhibited single RyR2s by a cooperative interaction, whereas Hill coefficients of ~1 argue against cooperative inhibition of [^{3}H]ryanodine binding to RyR2. The reasons for these differences are not clear but may be related to isoform-specific differences, the use of SR vesicles *versus* purified RyRs, or the absence of a membrane potential in [^{3}H]ryanodine binding but not single channel measurements. Another difference was that in the presence of AMPPCP, RR fully inhibited [^{3}H]ryanodine binding to RyR1 but not RyR2 at RR concentrations as high as 100 μM. Differences in the effectiveness of RR in inhibiting RyR isoforms were also noted in $^{45}Ca^{2+}$ uptake measurements using skeletal and cardiac SR vesicles and in single channel measurements using purified RyRs.

Ruthenium red has been extensively used as a diagnostic tool in single channel measurements of RyRs (2). In general, RR was applied to RyRs under conditions that favored full channel closings and disfavored the formation of substates. The present study defines conditions that result in the formation of cytosolic and lumenal RR-related substates in both RyR1 and RyR2. The majority of experiments were done in a symmetric KCl solution in the absence of a high lumenal Ca^{2+} concentration because it avoided the formation of a large Ca^{2+} gradient near the cytosolic channel pores (34), thereby simplifying analysis of the interaction of RyRs with RR. The RyR ion channels conduct Ca^{2+} across the SR membrane in muscle at a membrane potential that is likely close to 0 mV (36). The effects of RR on single channels were therefore also determined at 0 mV with 10 mM Ca^{2+} as the conducting ion. In both recording conditions, lumenal and cytosolic RR induced subconductance states. We found that probability of substate formation (P_{sub}) depended on cytosolic and lumenal ruthenium red concentration, P_o, and holding potential. Cytosolic RR induced a predominant substate in K^+-conducting channels at positive membrane potentials that favored cytosolic to lumenal cation fluxes. Substate formation was favored by conditions that resulted in nearly full channel activation. The most straightforward explanation is that cytosolic RR binds to sites located in the conductance pathways of RyR1 and RyR2 and that channel openings with long durations were required for RR to access these sites. The interaction of RyR2 with lumenal RR differed in several respects from that with cytosolic RR. First, lumenal [RR] >1 μM was required to induce full channel closings, suggesting the absence of high affinity lumenal regulatory sites for RR. Second, in contrast to cytosolic RR, lumenal RR induced a major subconductance in RyR2 at a negative holding potential. At a positive membrane potential, elevated levels of lumenal RR produced channel closings. However, these were too brief and poorly resolved at the time resolution of the lipid bilayer set-up to be further analyzed. Interaction of lumenal RR with RyR1 was more complex and induced three major substates. Substates were observed at negative and positive holding potentials, which suggested a low voltage dependence for their formation. Further studies are required to clarify the mechanism(s) of the formation of the RR-lumenal related RyR1 substates.

Ca^{2+}-conducting channels recorded at 0 mV formed substates with conductances similar to those formed by the K^+-conducting channels, with a $P_{sub} \leq 0.1$ at RR concentrations ≤500 nM. Higher concentrations caused complete channel closings in the majority of the experiments. Thus, the substates are likely of physiological relevance; however, the dominant mechanism of RR interaction with the Ca^{2+}-conducting RyRs appears to be full closure.

Ma (23) described the effects of RR on the ryanodine-modified skeletal RyR. Several cytosolic RR molecules produced an all-or-none flickery block with a Hill coefficient of 2. Lumenal RR created a different blocking effect by attenuating the single channel currents instead of forming a substate. These results suggested that different binding sites are located in the conduction pore of the ryanodine-modified skeletal muscle RyR. Ma (23) did not describe the effects of RR on ryanodine-unmodified RyR1 or RyR2.

Does RR reduce the channel conductance of the RyRs by partial occlusion of the channel pore, or are the subconductances the result of RR-dependent changes in channel protein conformation? For other ion channels, examples for both mechanisms exist (38–42). In the cardiac RyR, large cytosolic monovalent tetraalkyl ammonium cations produced a substate with a linear current-voltage relationship, a Hill coefficient of 1, and an effective gating charge of 1.7 (31). These results were explained in terms of a partial block in which the binding of more than one tetralkyl ammonium cation in the voltage drop of RyR2 produced an electrostatic barrier for ion translocation. The binding of the reversible ryanoid 21-amino-9α-hydroxyryanodine to a cytosolic site of the open RyR2 channel was strongly influenced by the membrane potential (43). The results suggested that the voltage dependence was due to a voltage-driven conformational change that altered the affinity of the binding site. Imperatoxin activator, a positively charged 33-amino acid peptide, induced a rectifying subconductance state by binding to a single cytosolic site of the cardiac and skeletal muscle RyRs (30). The formation of rectifying substates suggested that imperatoxin activator might have induced a conformational change in both RyRs. RR also induced rectifying subconductance states in the RyRs. The rate of formation but not the current amplitude of the substates was dependent on RR concentration. These results favor a conformational change as the mechanism for the formation of the substates. A conformational change can explain why the binding of one or more RR produces only one predominant substate.

Voltage dependence of substates suggests that RR binds to cytosolic and lumenal sites in the conductance pathway of RyR2. However, the current amplitudes of the cytosolic and lumenal RR-related substates were different, which argues against a common binding site. For the cytosolic RR binding site, an effective gating charge of 1.3 was determined. For the lumenal site, the gating charge was 0.8. Dividing these numbers by the six positive charges of RR yields an electrical distance of 0.22 from the cytosolic side and 0.13 from the lumenal side for the location of the RR binding sites in the voltage drop of the RyR2. The calculations are based on the assumption that all charges of RR enter the conduction pathway. The above numbers would be smaller if more than one RR molecule enters the conduction pathway. The RyRs consist of a large 29 × 29 × 12-nm cytosolic foot region with a large, centrally located vestibule and a smaller transmembrane region that extends ~7 nm toward the SR lumen (44, 45). Therefore, the total length of the conductance pathway may be 19 nm. By comparison, RR has an estimated length of 1.2 nm with a diameter of 0.4 nm. Accordingly, it is conceivable that several RRs simultaneously enter the conduction pathway of the tetrameric channel complexes. Theoretical considerations suggest that a significant portion of the voltage drop may occur in the vestibules of a channel (46). Thus, the RR binding sites may be close to the cytosolic and lumenal entrances of the conductance pathway.

In conclusion, RR modifies RyRs by at least two different

mechanisms. RR inhibits the Ca^{2+}-activated RyRs by a voltage-independent mechanism involving the noncompetitive interaction between Ca^{2+} regulatory and RR inhibition sites. In addition, cytosolic and lumenal RR can induce substates in RyRs. Formation of substates is influenced by membrane potential, and the rate of formation but not conductance of the substates is dependent on RR concentration. These observations argue against partial occlusion of the channel pore by RR. An alternative explanation is that the substates are the result of voltage- and RR-dependent changes in channel protein conformation. The formation of substates reduces the effectiveness of RR as an inhibitor of RyR channel activity. Therefore, caution is required when experiments are done under conditions that, as defined in this study, favor formation of these substates.

REFERENCES

1. Franzini-Armstrong, C., and Protasi, F. (1997) *Physiol. Rev.* **77,** 699–729
2. Zucchi, R., and Ronca-Testoni, S. (1997) *Pharmacol. Rev.* **49,** 1–51
3. Sutko, J. L., and Airey, J. A. (1996) *Physiol. Rev.* **76,** 1027–1071
4. Coronado, R., Morrissette, J., Sukhareva, M., and Vaughan, D. M. (1994) *Am. J. Physiol.* **266,** C1485–C1504
5. Meissner, G. (1994) *Annu. Rev. Physiol.* **56,** 485–508
6. McPherson, P. S., and Campbell, K. P. (1993) *J. Biol. Chem.* **268,** 13765–13768
7. Reed, K. C., and Bygrave, F. L. (1974) *FEBS Lett.* **46,** 109–114
8. Matlib, A. M., Zhou, Z., Knight, S., Ahmed, S., Choi, K. M., Krause-Bauer, J., Phillips, R., Altschuld, R., Katsube, Y., Sperelakis, N., and Bers, D. M. (1998) *J. Biol. Chem.* **273,** 10223–10231
9. Ohnishi, S. T. (1979) *J. Biochem.* **86,** 1147–1150
10. Miyamoto, H., and Racker, E. (1981) *FEBS Lett.* **133,** 235–238
11. Kim, D. H., Ohnishi, S. T., and Ikemoto, N. (1983) *J. Biol. Chem.* **258,** 9662–9668
12. Chamberlain, B., Volpe, P., and Fleischer, S. (1984) *J. Biol. Chem.* **259,** 7547–7553
13. Chu, A., Volpe, P., Costello, B., and Fleischer, S. (1986) *Biochemistry* **25,** 8315–8324
14. Meissner, G., and Henderson, J. S. (1987) *J. Biol. Chem.* **262,** 3065–3073
15. Palade, P. (1987) *J. Biol. Chem.* **262,** 6135–6141
16. Chu, A., Diaz-Munoz, M., Hawkes, M. J., Brush, K., and Hamilton, S. L. (1990) *Mol Pharm.* **37,** 735–741
17. Calviello, G., and Chiesi, M. (1989) *Biochemistry* **28,** 1301–1306
18. Zimanyi, I., and Pessah, I. N. (1991) *J. Pharmacol. Exp. Ther.* **256,** 938–946
19. Baylor, S. M., Hollingworth, S., and Marshall, M. W. (1989) *J. Physiol.* **408,** 617–635
20. Brunder, D. G., Gyorke, S., Dettbarn, C., and Palade, P. (1992) *J. Physiol.* **445,** 759–778
21. Smith, J. S., Coronado, R., and Meissner, G. (1985) *Nature* **316,** 446–449
22. Rousseau, E., Smith, J. S., Henderson, J. S., and Meissner, G. (1996) *Biophys. J.* **50,** 1009–1014
23. Ma, J. (1993) *J. Gen. Physiol.* **102,** 1031–1056
24. Meissner, G. (1984) *J. Biol. Chem.* **259,** 2365–2374
25. Lee, H.-B., Xu, L., and Meissner, G. (1994) *J. Biol. Chem.* **269,** 13305–13312
26. Jones, L. R., and Cala, S. E. (1981) *J. Biol. Chem.* **256,** 11809–11818
27. Fleischer, S., Ogunbunmi, E. M., Dixon, M. C., Fleer, E. A. M. (1995) *Proc. Natl. Acad Sci. U. S. A.* **82,** 7256–7259
28. Meissner, G. (1986) *J. Biol. Chem.* **261,** 6300–6306
29. Feher, J. J., LeBolt, W. R., and Manson, N. H. (1989) *Circ. Res.* **65,** 1400–1408
30. Tripathy, A., Resch, W., Xu, L., Valdivia, H. H., and Meissner, G. (1998) *J. Gen. Physiol* **111,** 679–690
31. Tinker, A., Lindsay, A. R. G., and Williams, A. J. (1992) *Biophys. J.* **61,** 1122–1132
32. Schoenmakers, J. M., Visser, G. J., Flick, G., and Theuvene, A. P. R. (1992) *BioTechniques* **12,** 870–879
33. Kargacin, G. J., Ali, Z., and Kargacin, M. E. (1998) *Pfluegers Arch.* **436,** 338–342
34. Xu, L., and Meissner, G. (1998) *Biophys. J.* **75,** 2302–2312
35. Tripathy, A., Xu, L., Mann, G., and Meissner, G. (1995) *Biophys. J.* **69,** 106–119
36. Meissner, G. (1983) *Mol. Cell. Biochem.* **55,** 65–82
37. Chen, S. R., and MacLennan, D. H. (1994) *J. Biol. Chem.* **269,** 22698–22704
38. Pietrobon, D., Prod'hom, B., and Hess, P. (1989) *J. Gen. Physiol.* **94,** 1–21
39. Prod'hom, B., Pietrobon, D., and Hess, P. (1987) *Nature* **329,** 243–246
40. Schild, L., Ravindran, A., and Moczydlowski, E. (1991) *J. Gen. Physiol.* **97,** 117–142
41. Strecker, G. J., and Jackson, M. B. (1989) *Biophys. J.* **89,** 795–806
42. Park, C. S., and Miller, C. (1992) *Neuron* **9,** 307–312
43. Tanna, B., Welch, W., Ruest, L., Sutko, J. L., and Williams, A. J. (1998) *J. Gen. Physiol.* **112,** 55–69
44. Radermacher, M., Rao, V., Grassucci, R., Frank, J., Timerman, A. P., Fleischer, S., and Wagenknecht, T. (1994) *J. Cell Biol.* **127,** 411–423
45. Serysheva, I. I., Orlova, E. V., Chiu, W., Sherman, M. B., Hamilton, S. L., and van Heel, M. (1995) *Nat. Struct. Biol.* **2,** 18–24
46. Jordan, P. C. (1986) in *Ion Channel Reconstitution* (Miller, C., ed) pp. 37–55, Plenum Press, New York